

K2-19, The first K2 multi-planetary system showing TTVs

S.C.C. Barros^{1,2}, J. M. Almenara^{3,4}, O. Demangeon¹, M. Tsantaki²,
A. Santerne², D. J. Armstrong⁵, D. Barrado⁶, D. Brown⁵,
M. Deleuil¹, J. Lillo-Box⁶, H. Osborn⁵, D. Pollacco⁵, L. Abe⁷,
P. Andre⁸, P. Bendjoya⁷, I. Boisse¹, A. S. Bonomo⁹, F. Bouchy¹,
G. Bruno¹, J. Rey Cerda¹⁰, B. Courcol¹, R. F. Díaz¹⁰,
G. Hébrard^{11,12}, J. Kirk⁵, J.C. Lachurié⁸, K. W. F. Lam⁵,
P. Martinez⁸, J. McCormac⁵, C. Moutou^{13,1}, A. Rajpurohit¹,
J.-P. Rivet⁷, J. Spake⁵, O. Suarez⁷, D. Toublanc^{8,14} and S. R. Walker⁵

¹Aix Marseille Université, CNRS, LAM (Laboratoire d'Astrophysique de Marseille) UMR 7326, 13388, Marseille, France email: susana.barros@astro.up.pt

²Instituto de Astrofísica e Ciências do Espaço, Universidade do Porto, CAUP, Rua das Estrelas, PT4150-762 Porto, Portugal

³Univ. Grenoble Alpes, IPAG, F-38000 Grenoble, France

⁴CNRS, IPAG, F-38000 Grenoble, France

⁵Department of Physics, University of Warwick, Gibbet Hill Road, Coventry, CV4 7AL, UK

⁶Departamento de Astrofísica, Centro de Astrobiología (CSIC-INTA), ESAC campus 28691 Villanueva de la Cañada (Madrid), Spain

⁷Laboratoire Lagrange, UMR7239, Université de Nice Sophia-Antipolis, CNRS, Observatoire de la Côte d'Azur, F-06300 Nice, France

⁸Observatoire de Belestia en Lauragais - Assoc. Astronomie Adagio 30 Route de Revel 31450 Varennes, France

⁹INAF - Osservatorio Astrofisico di Torino, via Osservatorio 20, 10025, Pino Torinese, Italy

¹⁰Observatoire Astronomique de l'Université de Genève, 51 chemin des Maillettes, 1290 Versoix, Switzerland

¹¹Institut d'Astrophysique de Paris, UMR7095 CNRS, Université Pierre & Marie Curie, 98bis boulevard Arago, 75014 Paris, France

¹²Observatoire de Haute-Provence, Université d'Aix-Marseille & CNRS, 04870 Saint Michel l'Observatoire, France

¹³CNRS, Canada-France-Hawaii Telescope Corporation, 65-1238 Mamalahoa Hwy., Kamuela, HI 96743, USA

¹⁴Université de Toulouse, UPS-CNRS, IRAP, 9 Av. colonel Roche, 31028 Toulouse, France

Abstract.

K2-19 is the second multi-planetary system discovered with K2 observations. The system is composed of two Neptune size planets close to the 3:2 mean-motion resonance. To better characterise the system we obtained two additional transit observations of K2-19b and five additional radial velocity observations. These were combined with K2 data and fitted simultaneously with the system dynamics (photo-dynamical model) which increases the precision of the transit time measurements. The higher transit time precision allows us to detect the chopping signal of the dynamic interaction of the planets that in turn permits to uniquely characterise the system. Although the reflex motion of the star was not detected, dynamic modelling of the system allowed us to derive planetary masses of $M_b = 44 \pm 12 M_\oplus$ and $M_c = 15.9 \pm 7.0 M_\oplus$ for the inner and the outer planets respectively, leading to densities close to Uranus. We also show that our method allows the derivation of mass ratios using only the 80 days of observations during the first campaign of K2.

Keywords. Planet detection, dynamical evolution and stability, K2-19, radial velocity

1. Introduction

Transit timing variations (TTVs) are caused by the mutual gravitational interaction of planets which perturb each others' orbit. These are larger when the planets are close to mean-motion resonances MMRs;. In near-resonant systems the resonant angles which measure the displacement of the longitude of the conjunction from the periapsis of each planet, circulate (or librate) over a period much longer than the orbital period of the outer planet, called the libration period or super period Lithwick et al. (2012). Analyses of the long term TTVs libration curve in *Kepler* transiting multi-planetary systems have allowed to derive dynamic planetary masses and helped confirm the planetary nature of many candidates.

After the failure of two out of four of the reaction wheels of the *Kepler* satellite the pointing accuracy was severely degraded. Cleaver engineering allowed the continuation of the mission in a new configuration named K2 Howell et al.(2014). K2 observes 4 fields a year close to the Ecliptic. The short duration of the observations of each field (~ 80 days) does not favour the detection of TTVs amongst planetary candidates discovered in these observations.

K2-19 (EPIC201505350) is a multi-planetary system detected in the K2 Campaign 1 (C1) data by Armstrong et al. (2015). The K2 observations show 2 transiting planets one with an orbital period $P_b \sim 7.92$ days and radius $R_b=7.23 \pm 0.60 R_{\oplus}$ and a companion close to the 3:2 MMR with an orbital period $P_c \sim 11.91$ days and radius $R_b = 4.21 \pm 0.31 R_{\oplus}$. The closeness to resonance implied that K2-19 was a good candidate for TTV and the brightness of the host star allowed follow-up transit observations from the ground. Approximately 200 days after the end of the K2 C1, a ground based transit was obtained showing TTVs of the inner planet with an amplitude of 1 hour, allowing the authors to validate the system. Here we present a photo-dynamical analysis of the K2-19 system and allow us to detect TTVs in the K2 data alone.

2. Method

2.1. Observations

K2-19 was observed during Campaign 1 of the K2 mission between 2014 June 3 and 2014 August 20 spanning ~ 80 days. We downloaded the pixel data from the Mikulski Archive for Space Telescopes (MAST)[†] and used a modified version of the CoRoT imagette pipeline Barros et al. (2014) to extract the light curve. We corrected the flux dependence with position due to the loss of pointing stability following Barros et al in prep.

Moreover, we obtained 3 ground based follow-up transits of K2-19. The first was taken on the 2015 February 28 with the 0.4-m Near Infrared Transiting ExoplanetS. The second was taken on 2015 March 8 with C2PU/Omicron telescope in Calern (Observatoire de la Cote d'Azur). Finally the third was taken on the 2015 March 16 with the Belestia 82-cm telescope.

Furthermore, we obtained 10 spectroscopic observations of K2-19 from 2015 February 21 to 2015 April 25 with the SOPHIE spectrograph mounted on the 1.93m telescope at the Observatoire de Haute-Provence Perruchot et al. (2011), Bouchy, et al.(2013). From these we derive radial velocities using a similar method to Santerne et al. (2012).

[†] http://archive.stsci.edu/kepler/data_search/search.php

Unfortunately, the radial velocity measurements are not precise enough to detect the stellar reflex velocity due to any of the planets. The spectroscopic observations were also used to derive the host stellar parameters following the methodology described in Tsantaki, et al. (2013). We obtained $T_{\text{eff}} = 5390 \pm 180$ K, $\log g = 4.42 \pm 0.34$ dex, $\xi_t = 1.02 \pm 0.24$ km s⁻¹, and $[Fe/H] = 0.19 \pm 0.12$ dex, hence it is a K-dwarf. These were used to derive the stellar mass and radius by interpolating the stellar evolution models using the MCMC described in Díaz et al. (2014). We obtained $M_* = 0.918_{-0.070}^{+0.086} M_{\odot}$ and $R_* = 0.926_{-0.069}^{+0.19} R_{\odot}$.

2.2. Photo-dynamical model

All the transits and radial velocities were modelled simultaneously with an n-body dynamical integrator that accounts for the gravitational interactions between all components of the system. We use the MERCURY n-body integrator Chambers (1999) to compute the 3 dimensional position and velocity of all system components as a function of time. We assume that only the host star and two planets are present. The stellar velocity projected onto the line-of-sight is used to model the observed radial velocities. To model the transits, we use the Mandel & Agol (2002) transit model parametrised by the planet-to-star radius ratio, quadratic limb darkening coefficients for each filter and using the sky projection of the planet-star separation computed from the output of MERCURY. This photo-dynamical model is coupled to a Monte Carlo Markov Chain (MCMC) routine, described in detail in Díaz et al. (2014), in order to derive the posterior distribution of the parameters.

To minimise correlations between the model parameters which prevent adequate exploration of the parameter space, we used the Huber et al. (2013) parametrisation (see Table 1). We run 46 independent MCMC chains and combined the results as described by Díaz et al. (2014) resulting in a final merged chain with 3500 independent points. Further details about the photo-dynamic method can be found in Almenara et al. (2015).

3. Results

The mode and the 68.3% confidence interval for the derived system parameters are given in Table 1. The inclination of planet c could not be constrained to either hemisphere. For clarity, in Table 1 we give only the solution where planet c orbits the same hemisphere as planet b. However, both values of the inclination: $88.92_{-0.41}^{+0.14}$ and $91.19_{0.14}^{+0.41}$ are equally probable.

3.1. Transit times

To derive the transit times, we calculate the mid point between the first and fourth transit contact using the MERCURY dynamic model output. Therefore, our transit time measurements include information on the system architecture and dynamics and as such are better constrained than direct measurement of the transit times in the light curve.

For comparison, we computed the transit times directly from the K2 light curves using a procedure similar to what is described in Barros, et al (2013). For each planet the transits were fitted simultaneously ensuring the same transit shape and we did not consider simultaneous transits. In Figure 1, we compare the derived transit times using the photo-dynamic model and the transit times derived with a standard procedure. To compute the ephemeris we use only the values of the observed transit times derived with the photo-dynamic model. For planet b we derived the ephemeris: T_b (BJD) = $7.921101(69) \times \text{Epoch} + 2456813.3767(21)$ and for planet c T_c (BJD) = $11.90727(58) \times \text{Epoch} + 2456817.2755(22)$.

Table 1. Model parameters. Posterior mode and 68.3% credible intervals. The orbital elements have the origin at the star (Asteroidal parameters in the MERCURY code) and are given for the reference time $t_{\text{ref}} = 2,456,813$ BJD.

Parameter	Mode and 68.3% credible interval	
	<i>Planet b</i>	<i>Planet c</i>
Semi-major axis, a [AU]	0.0762 ± 0.0022	0.1001 ± 0.0029
Eccentricity, e	$0.119^{+0.082}_{-0.035}$	$0.095^{+0.073}_{-0.035}$
Inclination, i [°]•	$88.87^{+0.16}_{-0.60}$	$88.92^{+0.14}_{-0.41}$ †
Argument of pericentre, ω [°]	179 ± 52	237^{+15}_{-68}
Longitude of the ascending node, n [°]•	180 (fixed)	$173.1^{+2.9}_{-5.6}$
Mean anomaly, M [°]	253^{+61}_{-27}	110^{+54}_{-34}
Radius ratio, R_p/R_\star •	$0.07451^{+0.0014}_{-0.00045}$	$0.04515 \pm 7.3 \times 10^{-4}$
Planet mass, M_p [M_\oplus]	44 ± 12	$15.9^{+7.7}_{-2.8}$
Planet radius, R_p [R_\oplus]	7.46 ± 0.76	4.51 ± 0.47
Planet density, ρ_p [$g\text{ cm}^{-3}$]	$0.492^{+0.26}_{-0.092}$	$0.94^{+0.46}_{-0.19}$
Planet surface gravity, $\log g_p$ [cgs]	$2.923^{+0.058}_{-0.17}$	$2.952^{+0.090}_{-0.15}$
α_1 [BJD-2,450,000]†•	$6813.38356 \pm 4.5 \times 10^{-4}$	6817.2732 ± 0.0013
α_2 [days]†•	$7.92008 \pm 4.0 \times 10^{-4}$	11.9068 ± 0.0013
$q_+ = \frac{M_{p,b} + M_{p,c}}{M_\star}$ •	$0.000198 \pm 4.7 \times 10^{-5}$	
$q_p = \frac{M_{p,c}}{M_{p,b}}$ •	0.42 ± 0.12	

• MCMC jump parameter

† reflected with respect to $i = 90^\circ$, the supplementary angle is equally probable.

* values for K2, NITES, C2PU, and Balesta respectively made to reduce the number of lines

‡ $\alpha_1 \equiv t_{\text{ref}} - \frac{\alpha_2}{2\pi} (M - E + e \sin E)$ with $E = 2 \arctan \left\{ \sqrt{\frac{1-e}{1+e}} \tan \left[\frac{1}{2} (\frac{\pi}{2} - \omega) \right] \right\}$; $\alpha_2 \equiv \sqrt{\frac{4\pi^2 a^3}{GM_\star}}$.

For each planet the respective and same ephemeris was subtracted from the transit times derived with both methods so that we could directly compare them.

We find that the difference of the transits times for both methods is less than 3σ hence the transit times from both methods agree. Using our photo-dynamic method, we obtain the double of the precision of the transit times as compared to the traditional method that does not include the dynamical constrains. For the K2-19 system the difference increases the significance of the TTVs for planet b and planet c, even in the short duration of the K2 observations, allowing us to better constraint the system architecture.

Armstrong et al. (2015) predicted that the resonant timescale of the system is ~ 5 years and hence it is not detectable with the current observation baseline and hence the phase curve cannot be used to constrain the planetary masses e.g. Lithwick et al. (2012). However, we detected the short period chopping signal at the much shorter synodic timescale. This chopping is clearly visible in Figure 1, every 3 orbits of planet b it has a close encounter with planet c that changes its orbit and the transit times. In the same figure the chopping is also seen for K2-19c. Probably the closest encounter of both planets happens near the transit time since planet c and planet b show simultaneous transits during the K2 observations.

In our case the detection of the chopping signal at the short synodic timescale allows us to directly determine planetary masses. This can be intuitively understood using the equations derived by Nesvorný & Vokrouhlický (2014), Deck & Agol (2015) although our system might not obey their model assumptions. However, as expected, without the detection of the libration period the orbital eccentricities are poorly constrained. To illustrate our uncertainty in the libration period and estimate an ephemeris for the system we evolved 1000 random steps of our MCMC chain till the end of 2015 shown In

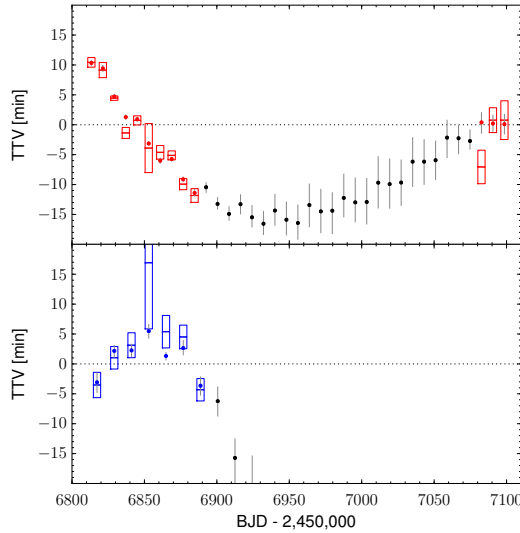


Figure 1. Comparison of the TTVs derived by the photo-dynamic model (as circles) with TTVs derived using a standard transit fitting (as boxes with the size of the 1 sigma error) for planet b (top panel) and planet c (bottom panel). For each planet we use the respective ephemeris derived using the photo-dynamic estimated values of only the observed transits which are marked in red for planet b and in blue for planet c.

Figure 2. It is clear that we cannot predict the transit times with good accuracy further than 200 days into the future. This is because of the uncertainty in the system parameters and the fact that we do not sample the full libration cycle. Noteworthy is the different shape of the TTVs of K2-19c in Figures 1 and 2. This is due to the different ephemeris (especially the mean period) used to calculate the TTVs. In each case the ephemeris was calculated from different sets of transits times, for Figure 1 we use only the observed transits while for Figure 2 we used all the times presented in that figure. Since the duration of the observations for K2 is too short to sample the resonant timescale, the period measured from K2 observations can be significantly different from the mean period of the system which can only be observationally probed with a much longer time span of the observation.

Finally, we use the photo-dynamic model described above fitting only the K2 light curve and using neither radial velocity nor ground-based transits nor stellar priors. As expected, the derived parameter distributions are wider, however we still find the best solution in agreement with the previous results. In particular the mass ratios are very well constrained $q_+ = 0.000159^{+0.000075}_{-0.000018}$ and $q_p = 0.481^{+0.24}_{-0.076}$. The TTVs derived using only the K2 observations show a clear chopping signal. So this method will be useful for short duration observations like K2, TESS and CHEOPS.

4. Take home messages

- Applying a photodynamical model leads to a better constrain on the system parameters compared with traditional TTV methods.
- Detecting short period TTVs (chopping) in K2-19 allowed to constrain the system without long time coverage. This will be very important for the analysis of the short duration K2 data and future observations with CHEOPS and TESS

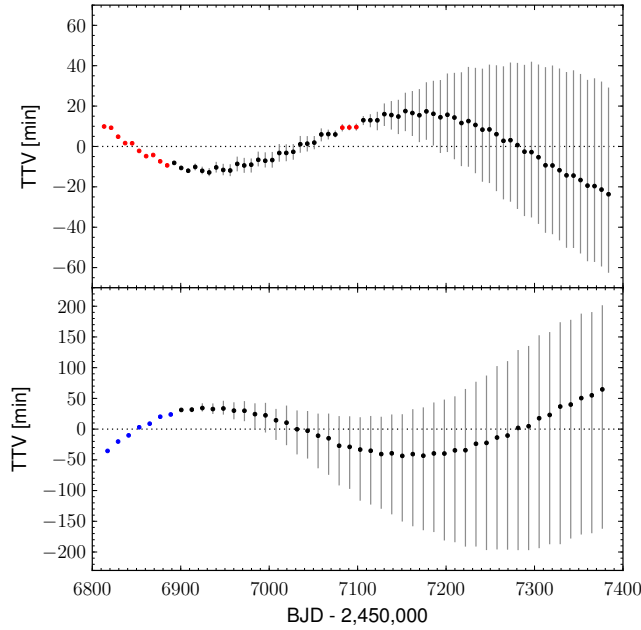


Figure 2. Prediction of the TTVs according to the photo-dynamic model until the end of 2015 for planet b (top panel) and planet c (bottom panel). For each planet we use the respective ephemeris derived from the points plotted. For K2-19b the chopping signal is also visible in this figure. Three transits are nearly on a linear ephemeris and there is an offset from the next three transits due to the conjunctions with the outer planet.

References

- Agol E., et al. 2005, *MNRAS*, 359, 567
 Almenara J. M. et al. , 2015, *MNRAS*, in press
 Armstrong D. J., et al., 2015a, *MNRAS*, in press
 Barros S. C. C., et al, 2013, *MNRAS* 430, 3032
 Barros S. C. C., et al., 2014, *A&A* 569, A74
 Borucki W. J., et al., 2010, *Science* 327, 977
 Bouchy F., et al., 2009, *A&A* 505, 853
 Bouchy F. et al. 2013, *A&A* 549, A49
 Chambers J. E., 1999, *MNRAS* 304, 793
 Deck K. M., Agol E., 2015, *ApJ* 802, 116
 Díaz R. F., et al. 2014, *MNRAS* 441, 983
 Holman M. J., et al., 2010, *Science* 1195778
 Howell S. B., et al., 2014, *PASP* 126, 398
 Huber D., et al., 2013, *Science* 342, 331
 Lithwick Y., Wu Y., 2012, *ApJL* 756, L11
 Lithwick Y., Xie J., Wu Y., 2012, *ApJ* 761, 122
 Mandel K., Agol E., 2002, 580, L171
 Nesvorný D., Beaugé C., 2010, *ApJL* ,709, L44
 Nesvorný D., Vokrouhlický D., 2014, *ApJ* 790, 58
 Nesvorný D. et al. 2012, *Science* 336, 1133
 Perruchot S., et al., 2011, in *Society of Photo-Optical Instrumentation Engineers (SPIE) Conference Series*. p. 15
 Santerne A., et al., 2012, *A&A* 545, A76
 Tsantaki M. et. al. 2013, *A&A* 555, A150